

Chapter 3: Observations: Surface and Atmospheric Climate Change

Coordinating Lead Authors: Kevin E. Trenberth, Philip D. Jones

Lead Authors: Peter G. Ambenje, Roxana Bojariu, David R. Easterling, Albert M. G. Klein Tank, David E. Parker, James A. Renwick, Fatemeh Rahimzadeh, Matilde M. Rusticucci, Brian J. Soden, Pan-Mao Zhai

Contributing Authors: Robert Adler, Lisa Alexander, Hans Alexandersson, Richard P. Allan, Mark P. Baldwin, Martin Beniston, David H. Bromwich, Inés Camilloni, Christophe Cassou, Daniel R. Cayan, Edmund K. M. Chang, John R. Christy, Aiguo Dai, Clara Deser, Nikolai Dotzek, John Fasullo, Ryan L. Fogt, Christopher K. Folland, Piers Forster, Melissa Free, Christoph Frei, Byron Gleason, Jürgen Grieser, Pavel Y. Groisman, Sergey K. Gulev, James W. Hurrell, Masayoshi Ishii, Simon A. Josey, Per W. Kållberg, George N. Kiladis, Ramesh H. Kripalani, Kenneth E. Kunkel, Chiu Ying Lam, John R. Lanzante, Jay H. Lawrimore, David H. Levinson, Beate G. Liepert, Gareth J. Marshall, Carl A. Mears, Philip W. Mote, Hishashi Nakamura, Neville Nicholls, Joel R. Norris, Taikan Oki, Franklin R. Robertson, Karen H. Rosenlof, Fred H. Semazzi, Dennis J. Shea, J. Marshall Shepherd, Theodore G. Shepherd, Steven C. Sherwood, Adrian J. Simmons, Ian Simmonds, Peter C. Siegmund, Chris D. Thorncroft, Peter W. Thorne, Sakari M. Uppala, Russell S. Vose, Bin Wang, Stephen G. Warren, Richard Washington, Matthew C. Wheeler, Bruce A. Wielicki, Takmeng Wong, David B. Wueertz.

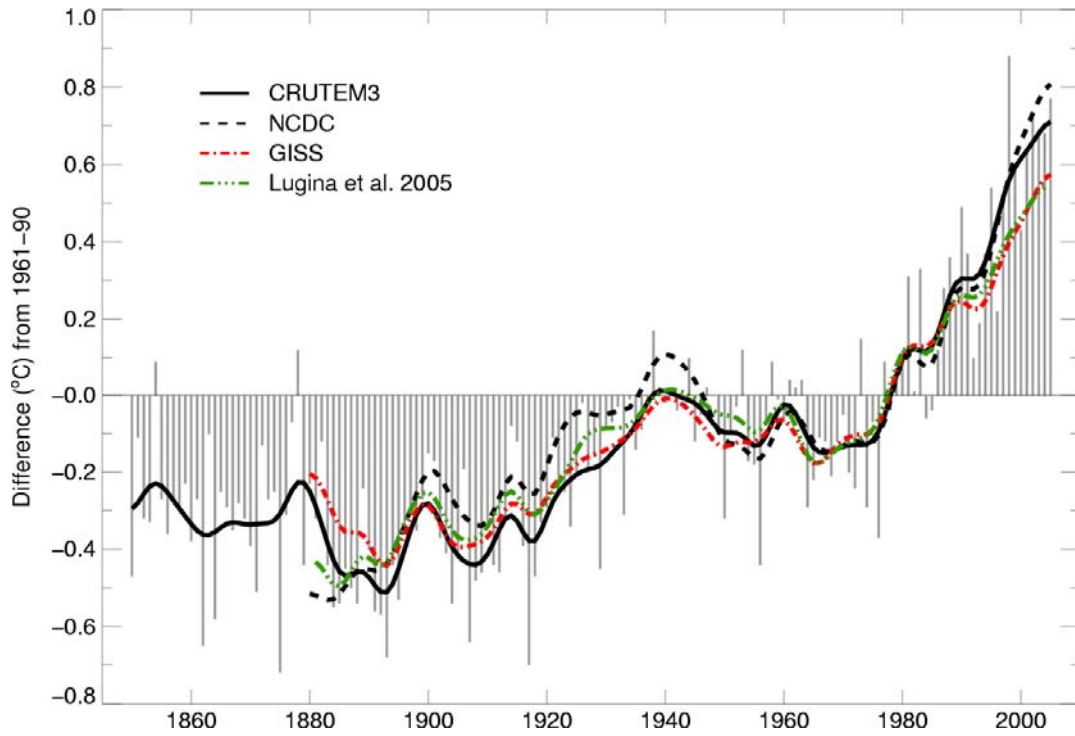
Review Editors: Brian J. Hoskins, Bubu P. Jallow, Thomas R. Karl

Date of Draft: 22 February 2006:

Notes: This is the TSU compiled version. All figures are designed for single column presentation (e.g., Figures 3.2.1, 3.2.9, 3.4.3, 3.4.5, etc.) or full page width (e.g., Figures 3.2.10, Question 3.1, Figure 1). The latter applies for panels aligned side by side (e.g., Figures 3.2.4, 3.2.5) and for the major assemblages Figures 3.3.3 and 3.8.3. Figure 3.3.3 will appear sideways, as given here. Otherwise, the figures should fit in a single column.

1 **Figures**

2



3

4

5

6

7

8

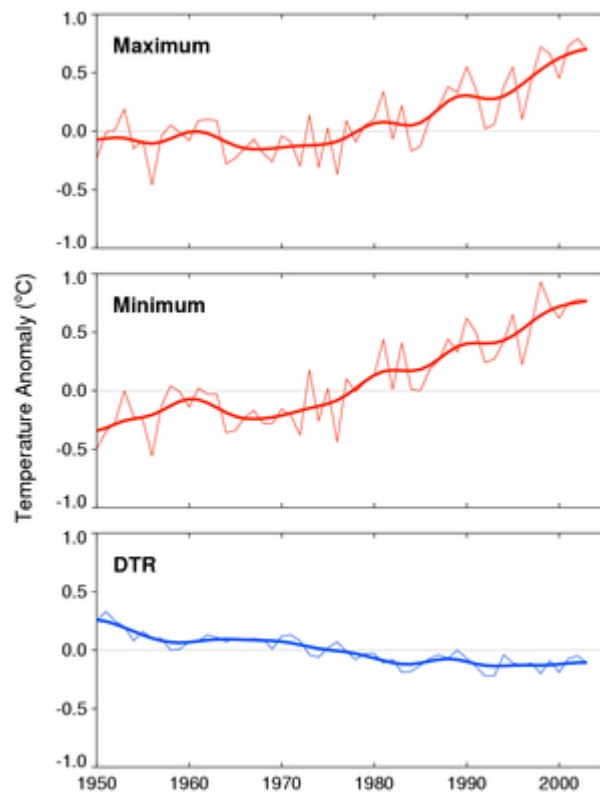
9

10

11

Figure 3.2.1. Annual anomalies of global land surface air temperature, 1861 to 2005, relative to the 1961–1990 mean (°C) for CRUTEM3 updated from Brohan et al. (2006). The smooth curves depict decadal variations (see Appendix 3.A). The thick solid black curve from CRUTEM3 is compared with those from NCDC (Smith and Reynolds, 2005) (black dashed) and GISS (Hansen et al., 2001) (red dashed) and Lugina et al. (2005) (green dashed).

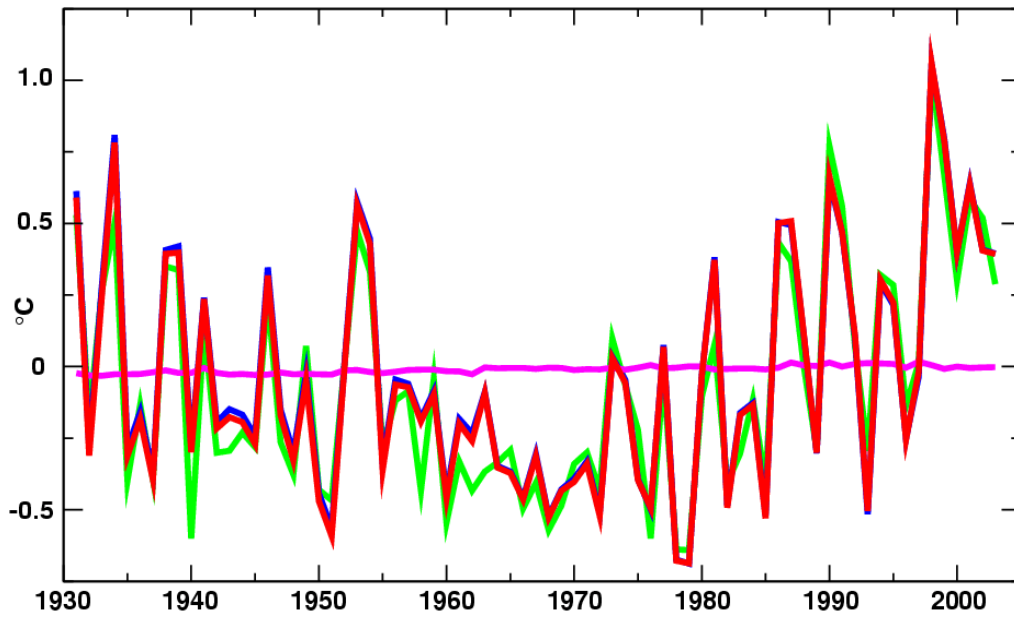
1
2



3
4
5
6
7
8
9

Figure 3.2.2. Annual anomalies relative to the 1961–1990 mean of maximum and minimum temperatures and diurnal temperature range (°C) averaged for the 71% of global land areas where data are available for 1950 to 2004. The smoothed curve shows the decadal variability (Appendix 3.A). Adapted from Vose et al. (2005a).

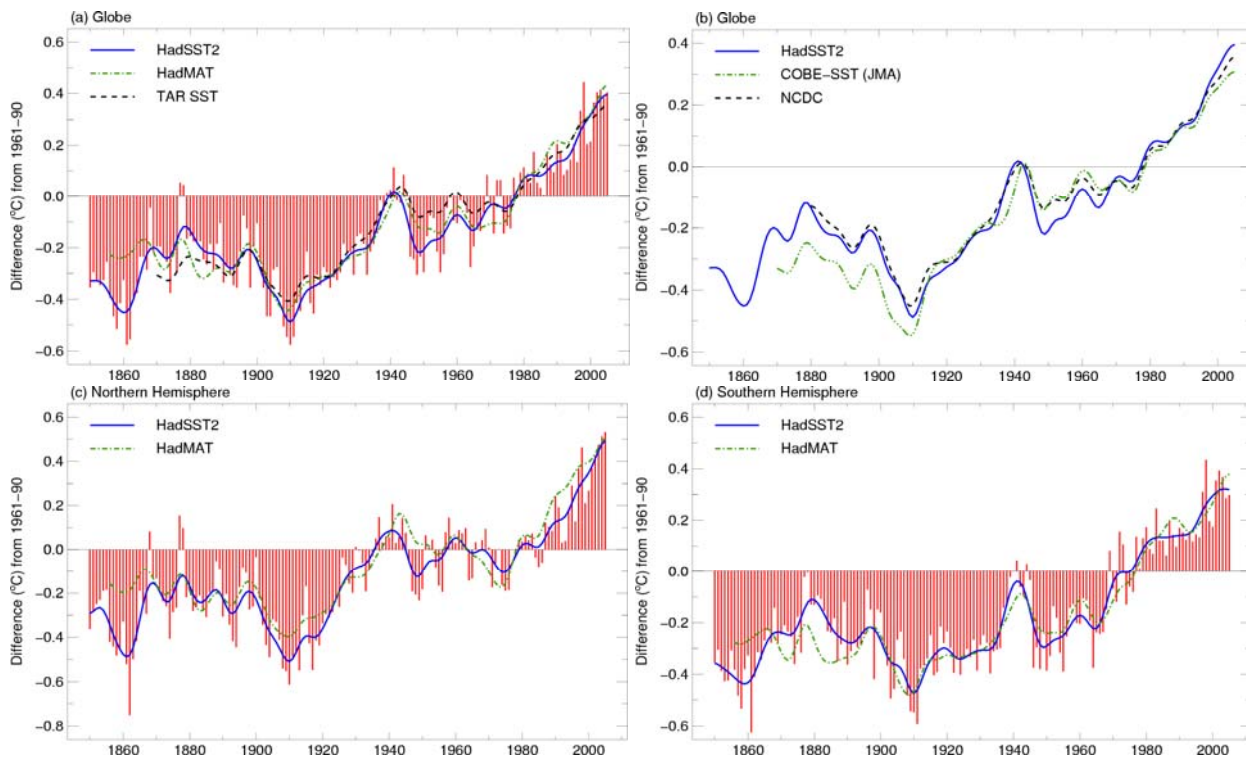
1
2



3
4
5
6
7
8
9
10
11

Figure 3.2.3. Anomaly ($^{\circ}\text{C}$) time series relative to the 1961-90 mean of the full USHCN data (red), the USHCN data without the 16% of the stations with populations of over 30,000 within 6 km in the year 2000 (blue), and the 16% of the stations with populations over 30,000 (green). The full USHCN set minus the set without the most urban stations is shown in magenta. Both the full data set and the data set without the high population stations had stations in all of the 2.5° latitude by 3.5° longitude grid boxes during the entire period plotted but the subset of high population stations only had data in 56% of these grid boxes.

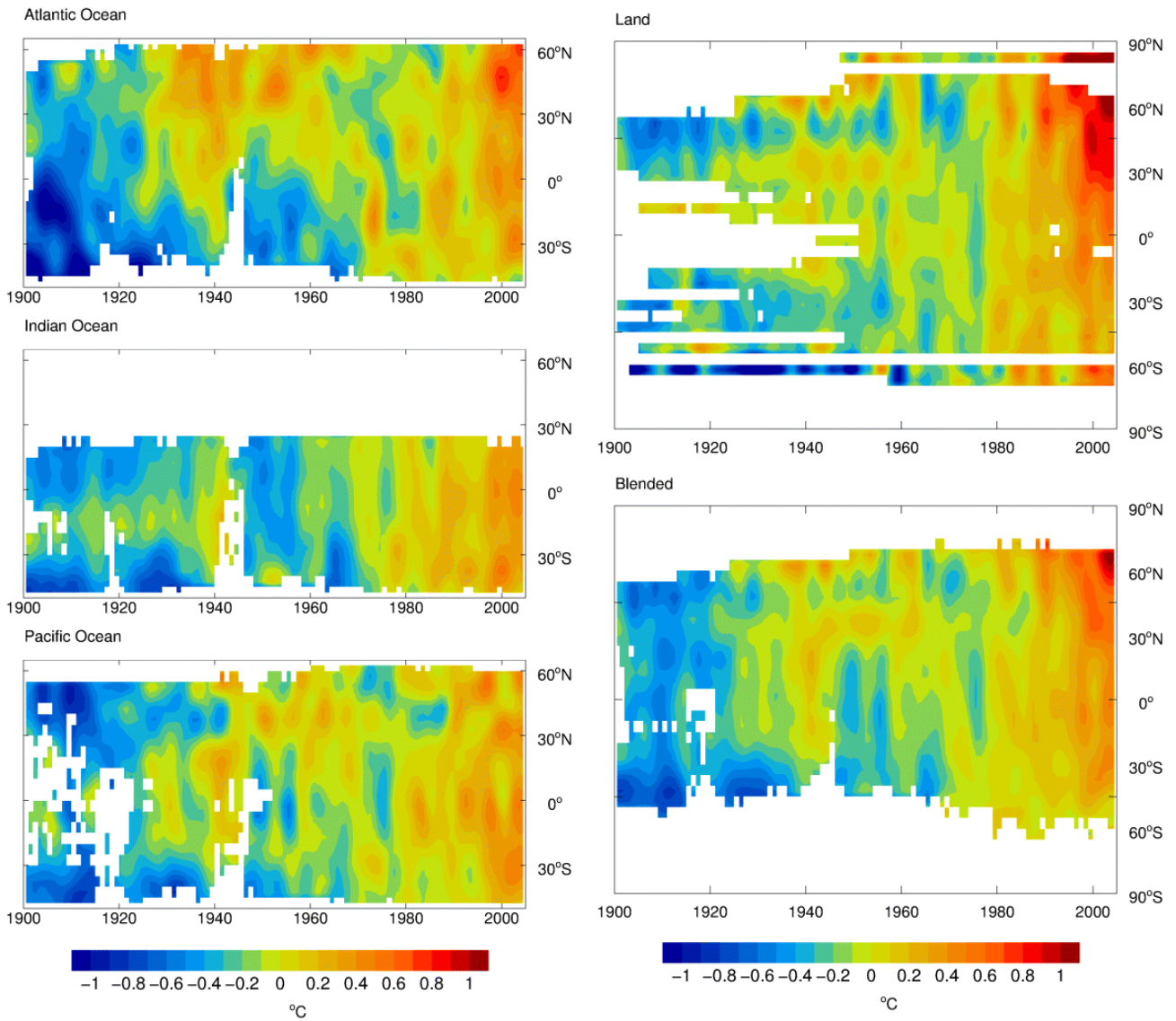
1
2



3
4
5
6
7
8
9
10
11
12

Figure 3.2.4. (a) Annual anomalies of global SST (HadSST2; red bars and blue solid curve) and global night marine air temperature (HadMAT, dotted green curve), 1850 to 2005, relative to the 1961–1990 mean (°C) from UKMO (Rayner et al., 2006). The decadal filter (Appendix 3.A) provides the smoothed curves. The dashed black curve shows equivalent smoothed SST anomalies from the TAR. (b) Smoothed annual global SST 1850 to 2005, relative to 1961–1990 (°C), from HadSST2 (thick blue line as in a) and from Reynolds et al. (2002) (NCDC; dashed black line, includes satellite data), and from Japan [(Ishii et al., 2005) COBE-SST (JMA)], green dashed line. These latter two series and HadMAT begin later in the 19th century than HadSST2. (c, d) as in (a) but for the NH and SH showing only the UKMO (Rayner et al., 2006) series.

1



2

3

4

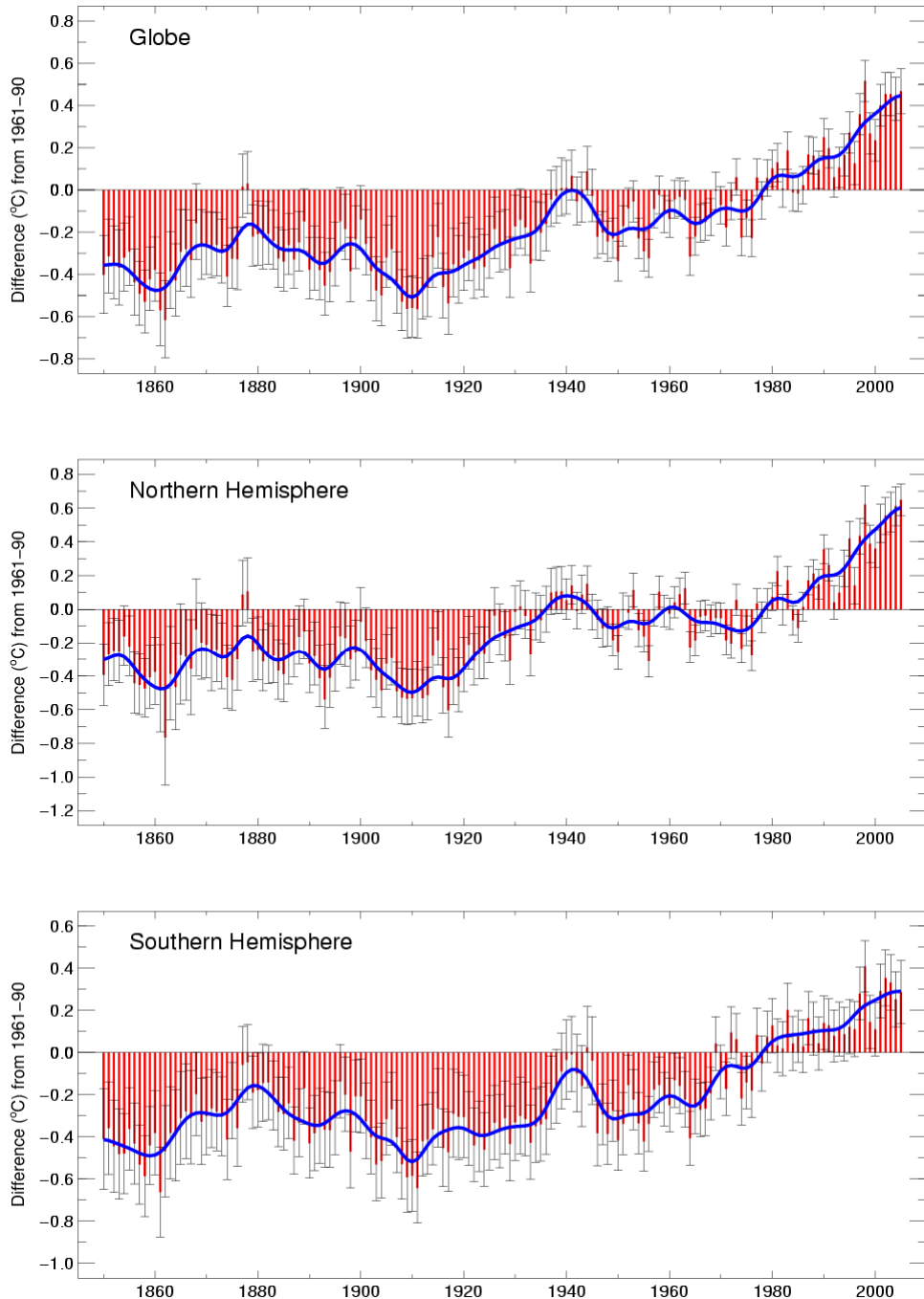
5

6

7

Figure 3.2.5. Latitude-time sections of zonal mean temperature from 1900 to 2005, relative to the 1961–1990 mean (°C). Left panels: SST annual anomalies across each ocean from HadSST2 (Rayner et al., 2006). Right panels: Surface temperature annual anomalies for land (top, CRUTEM3) and land plus ocean (bottom, HadCRUT3). The values are smoothed with a 1/12(1–3–4–3–1) filter to remove fluctuations less than 6 years or so (see Appendix 3.A) and missing data are white.

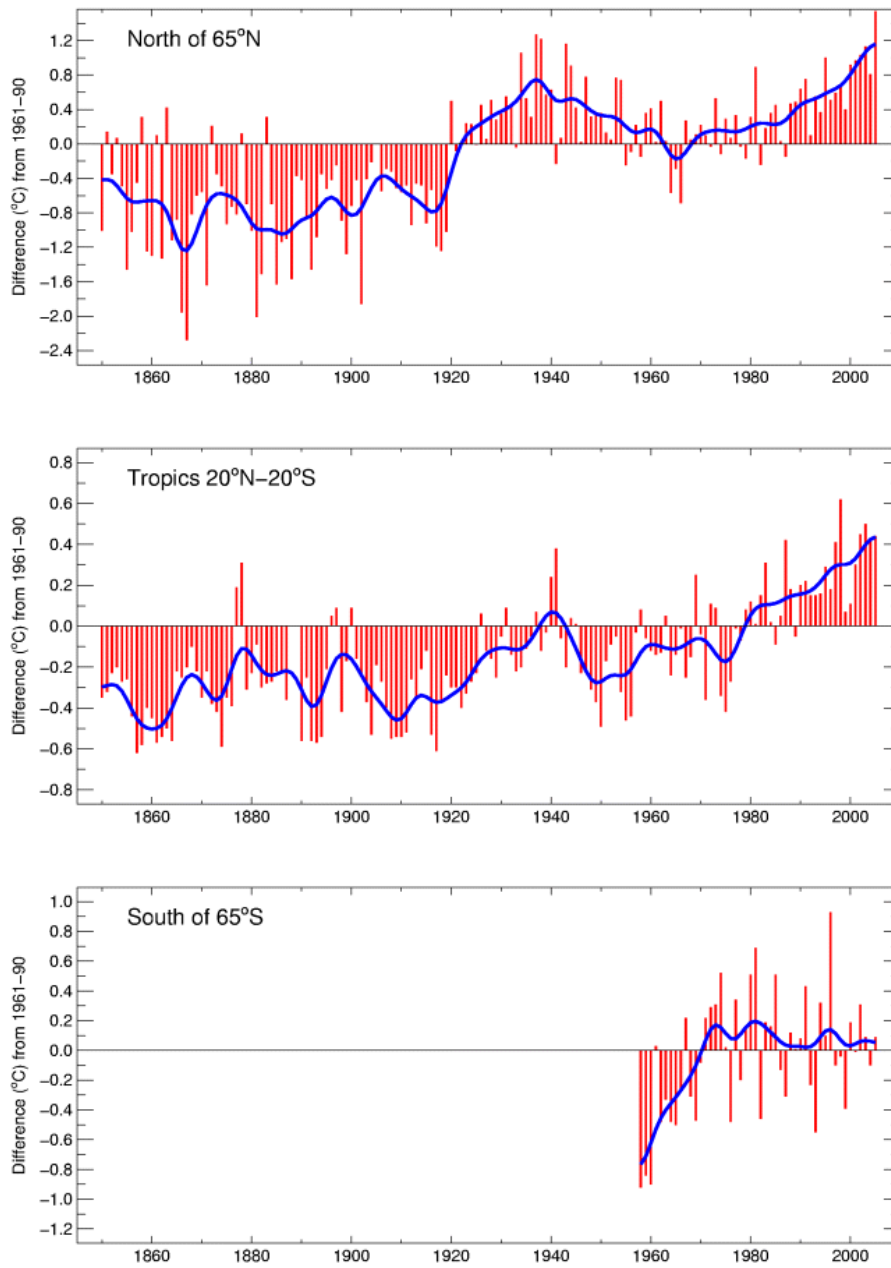
1
2



3
4
5
6
7

Figure 3.2.6. Global and hemispheric annual combined land surface air temperature and SST (°C) (red) relative to the 1961–1990 mean, along with ± 2 standard error ranges, from HadCRUT3 (Brohan et al., 2006). The blue decadal smoothing is described in Appendix 3.A.

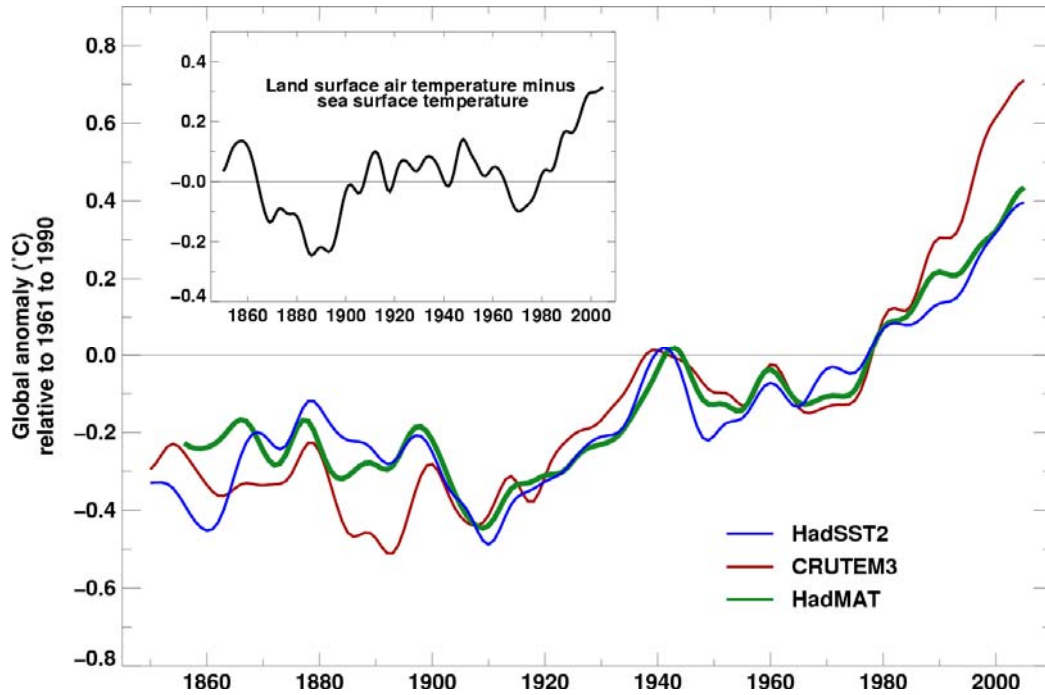
1
2



3
4
5
6
7

Figure 3.2.7. Annual combined land surface air temperature and SST (°C), relative to the 1961–1990 mean, from HADCRUT3 (Brohan et al., 2006) for the tropics (20°N–20°S), and polar regions north and south of 65°. Blue decadal smoothing is described in Appendix 3.A.

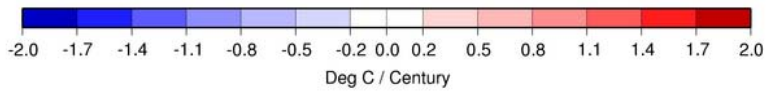
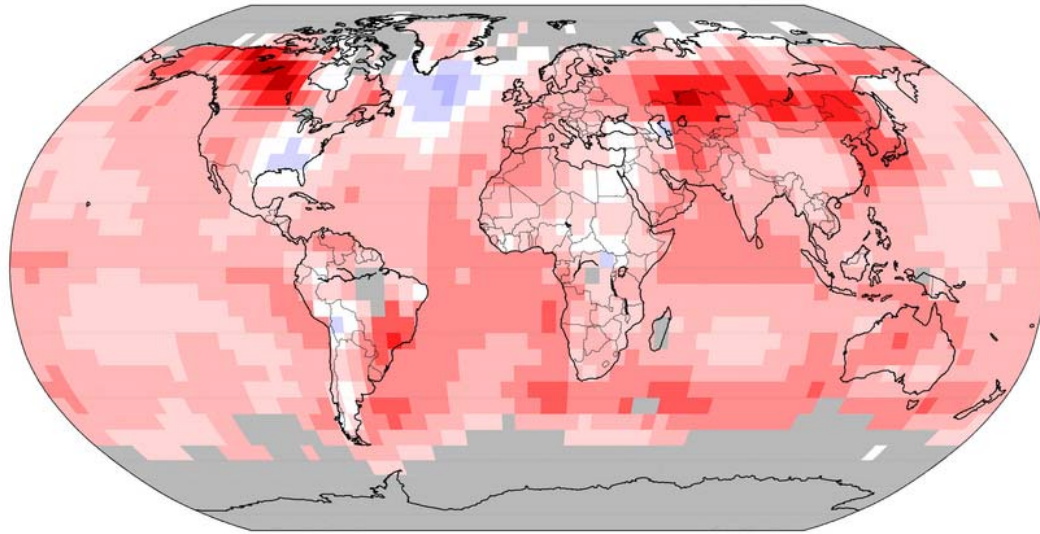
1
2



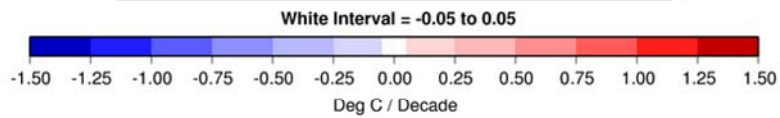
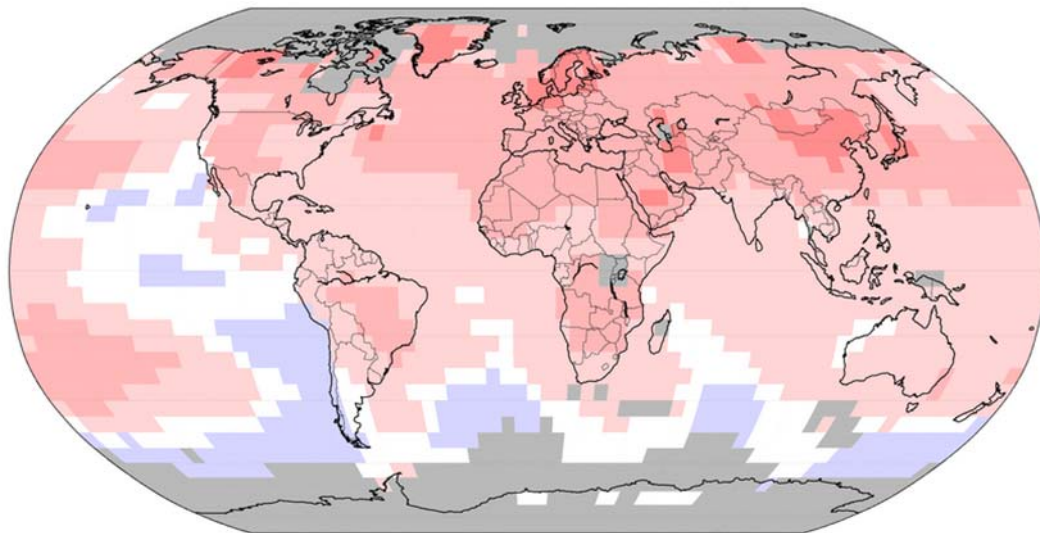
3
4
5
6
7
8
9

Figure 3.2.8. Smoothed annual anomalies of global average sea surface temperature (blue curve), night marine air temperature (green curve) and land surface air temperature (red curve) 1861 to 2005, relative to their 1961–1990 means (°C) (Rayner et al., 2006; Brohan et al., 2006). Also shown (inset) are the smoothed differences between the land-surface air and SST anomalies (i.e., red minus blue).

1
2



3

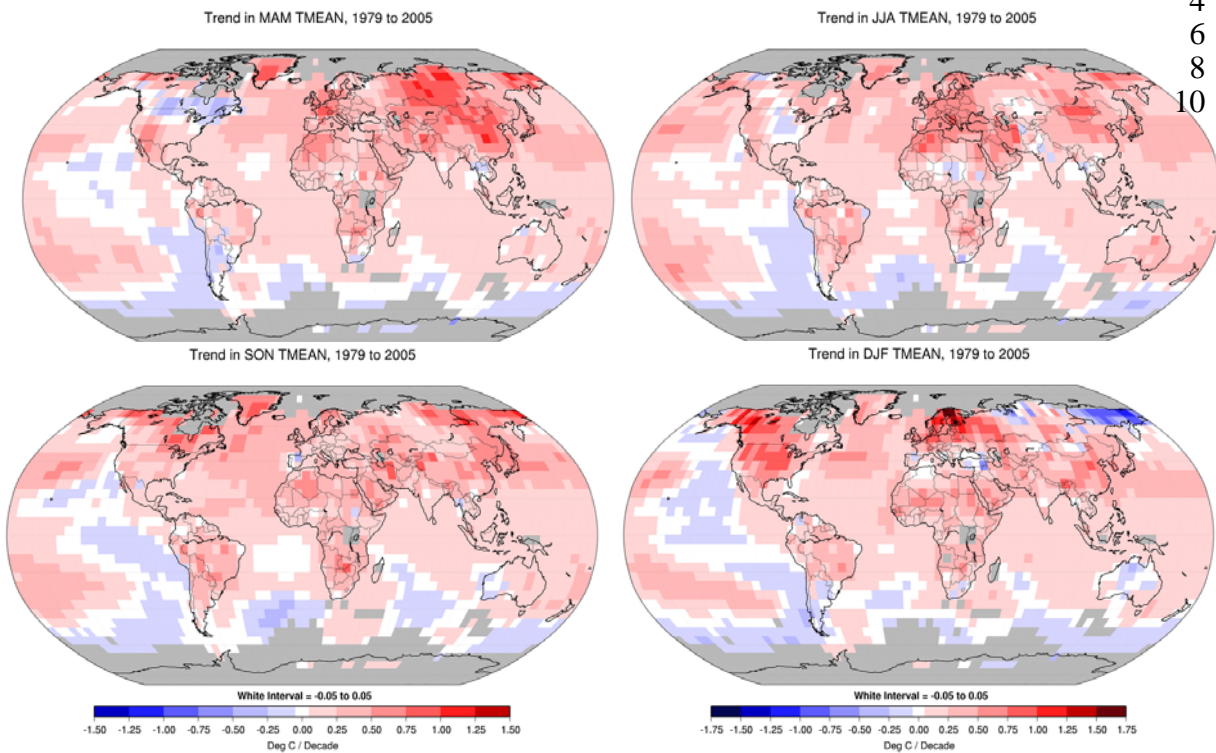


4
5
6
7
8
9
10
11

Figure 3.2.9. Linear trend of annual temperatures for 1901–2005 (upper; °C century⁻¹) and 1979–2005 (lower; °C decade⁻¹). Areas in grey have insufficient data to produce reliable trends. The minimum number of years needed to calculate a trend value is 66 years for 1901–2005 period and 18 years for 1979–2005. An annual value is available if there are 10 valid monthly temperature anomaly values. The dataset used was produced by NCDC from Smith and Reynolds (2005).

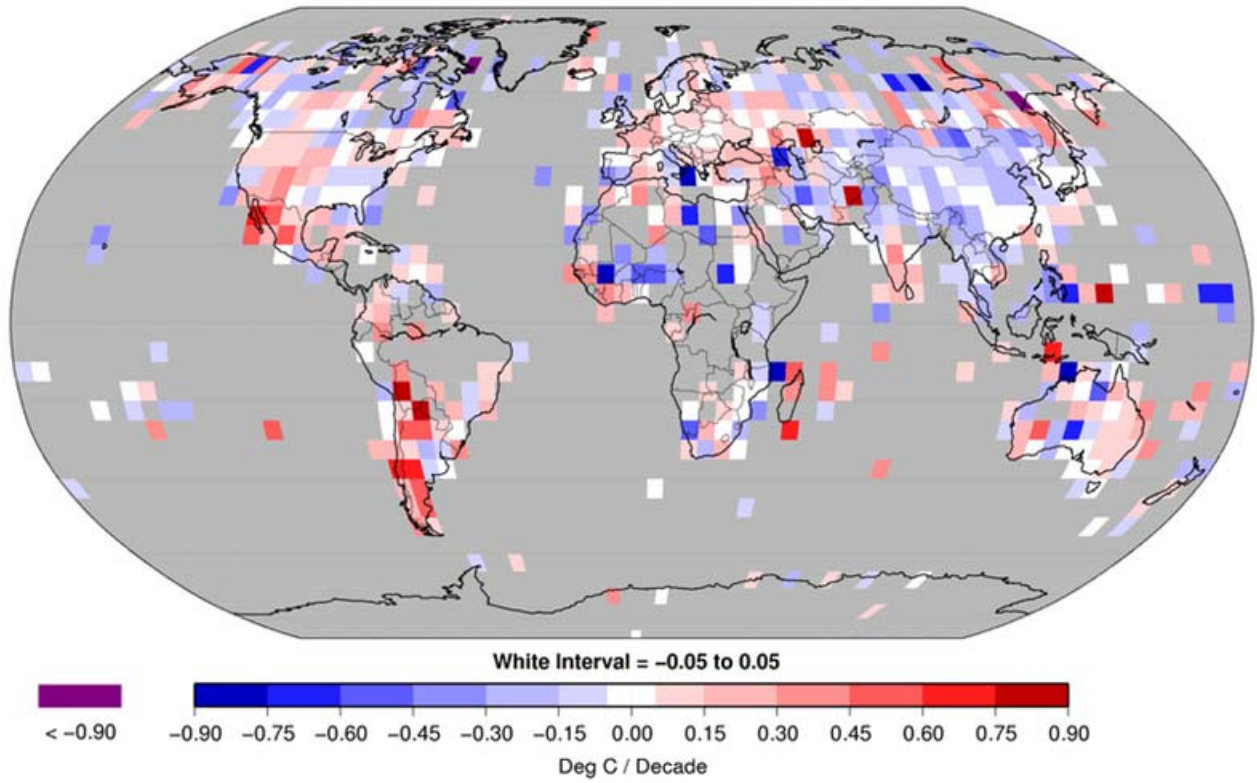
1
2

4
6
8
10



11 **Figure 3.2.10.** Linear trend of seasonal MAM, JJA, SON and DJF temperature for 1979–2005. The units are
 12 °C decade⁻¹. Areas in grey have insufficient data to produce reliable trends. The minimum number of years
 13 to calculate a trend value is 18. A seasonal value is available if there are 2 valid monthly temperature
 14 anomaly values. The dataset used was produced by NCDC from Smith and Reynolds (2005).
 15

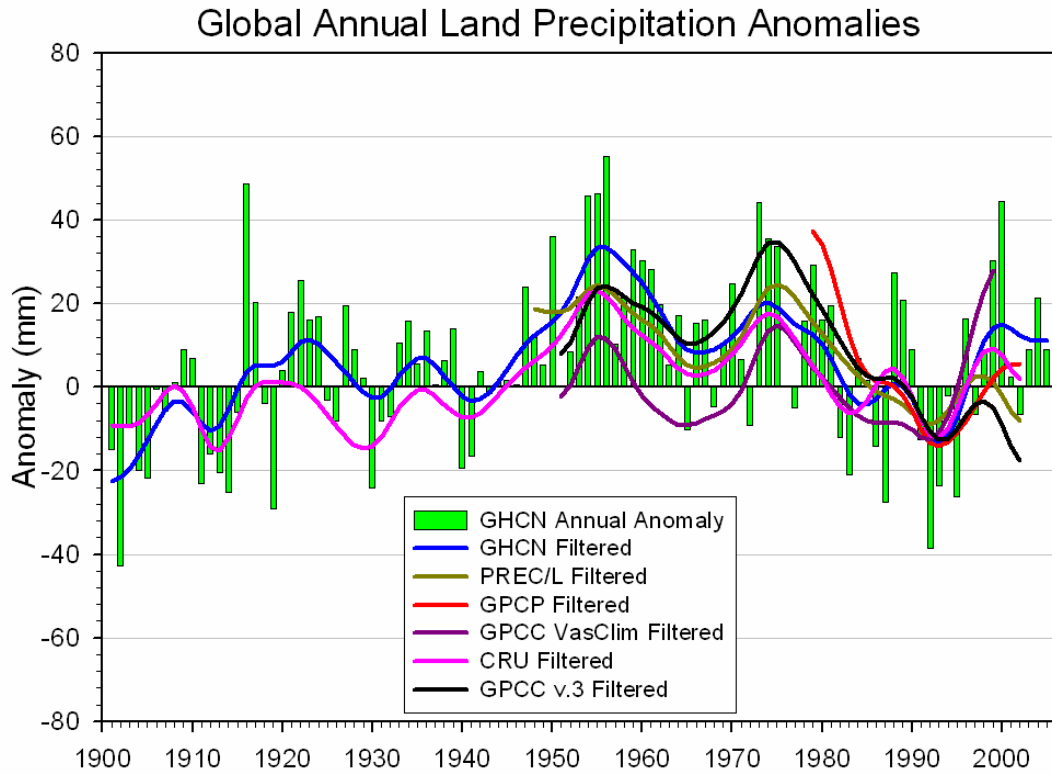
1
2



3
4
5
6
7

Figure 3.2.11. Linear trend in annual mean DTR for 1979 to 2004 in $^{\circ}\text{C decade}^{-1}$. Grey regions indicate incomplete or missing data. After Vose et al. (2005a).

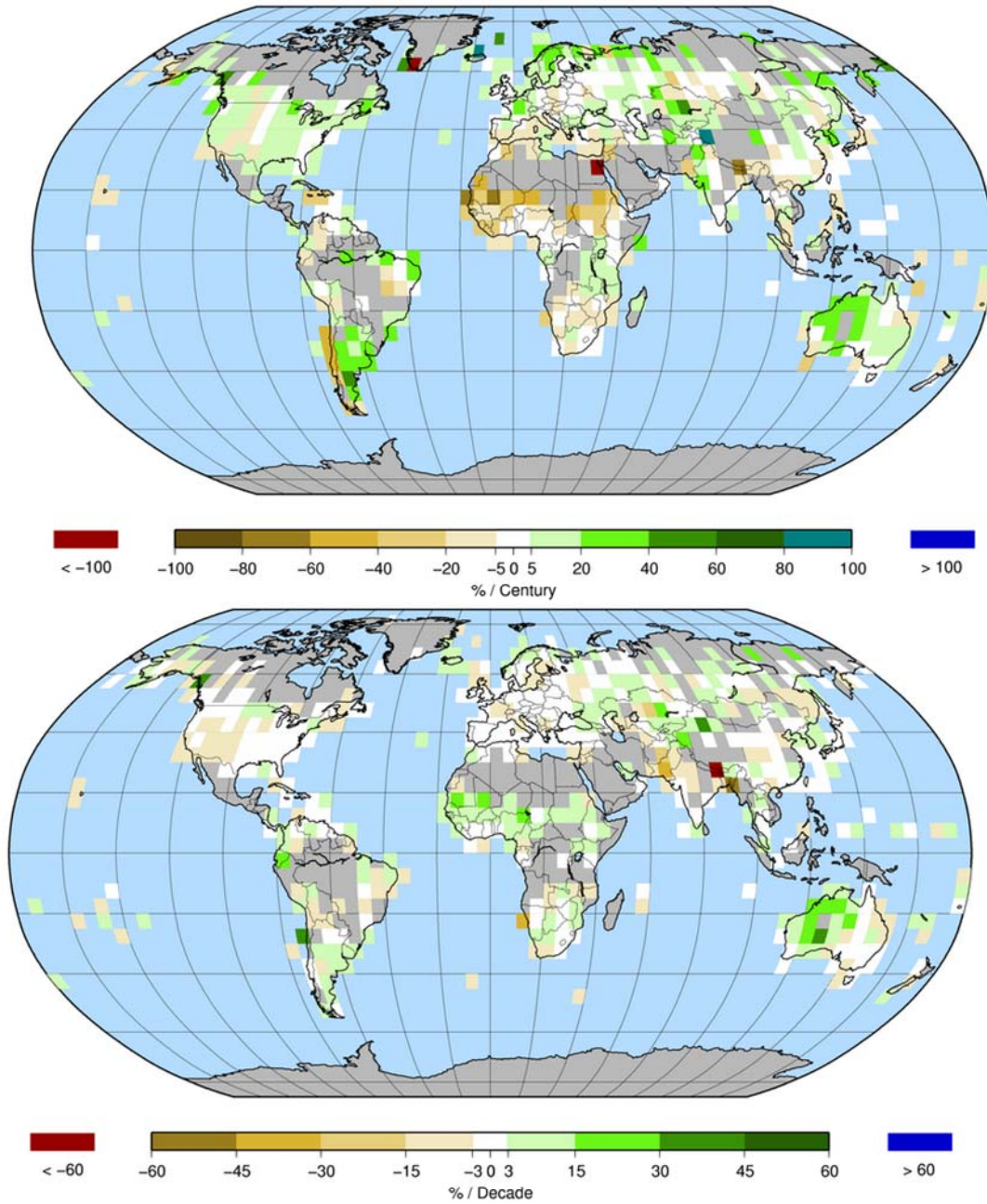
1
2



3
4
5
6
7
8
9

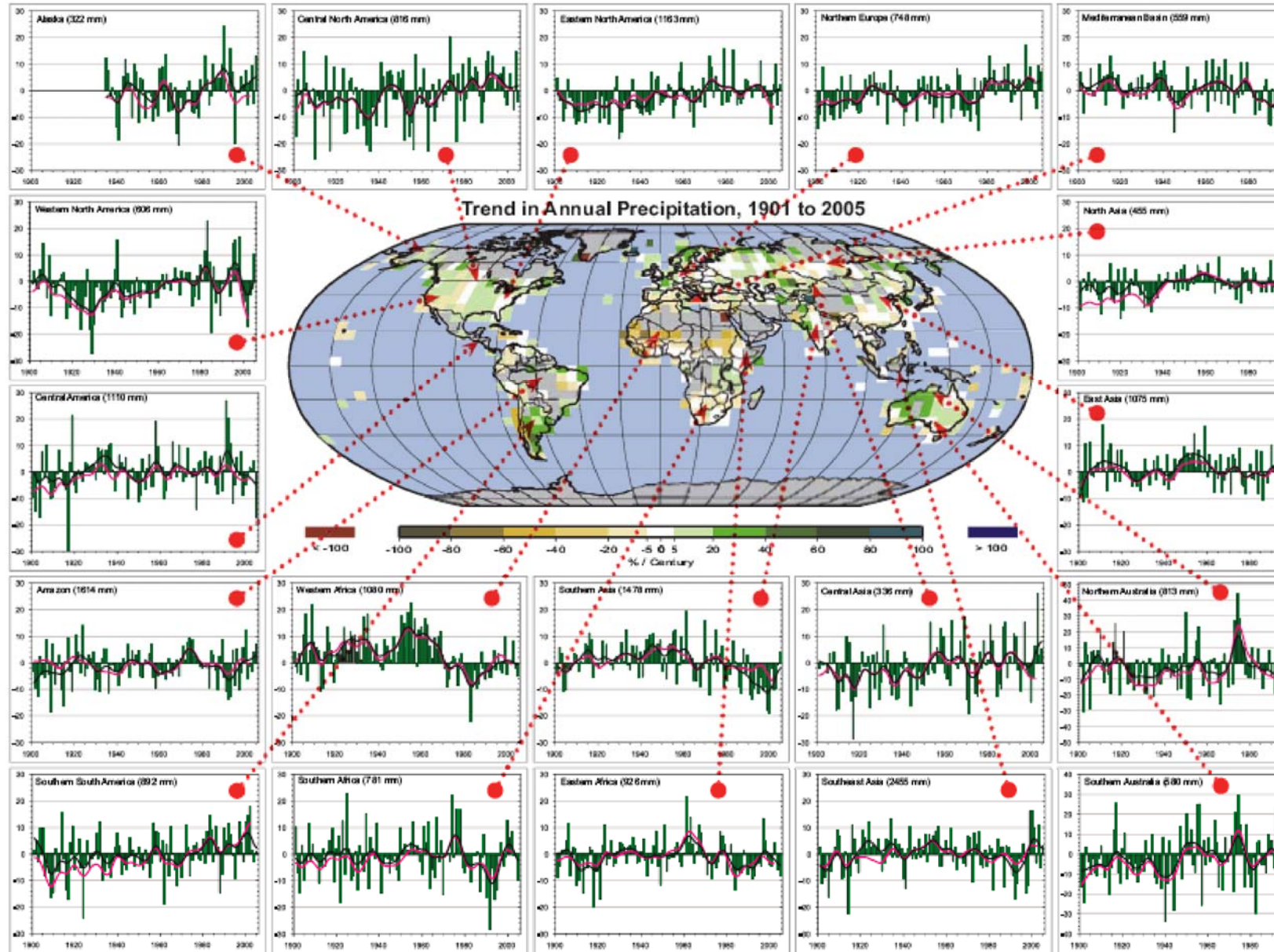
Figure 3.3.1. Time series for 1900 to 2005 of annual global land precipitation anomalies from GHCN with respect to the 1981–2000 base period (to convert to mm/day divide by 365 or 366). Smoothed values (using the decadal filter in Appendix 3.A) are also given for the GHCN (Peterson and Vose, 1997), PREC/L (Chen et al. (2002)), GPCP (Adler et al., 2003), GPCC (Rudolf et al., 1994) and CRU (Mitchell and Jones, 2005).

1



2 **Figure 3.3.2.** Trend of annual precipitation amounts for 1901–2005 (upper, % century⁻¹) and 1979–2005
 3 (lower, % decade⁻¹) the percentage being based on the 1961–90 period. Areas in grey have insufficient data
 4 to produce reliable trends. The minimum number of years to calculate a trend value is 66 for 1901–2005
 5 period and 18 for 1979–2005. An annual value is complete for a given year if all twelve monthly percentage
 6 anomaly values are present. The GHCN precipitation dataset from NCDC was used.
 7 .

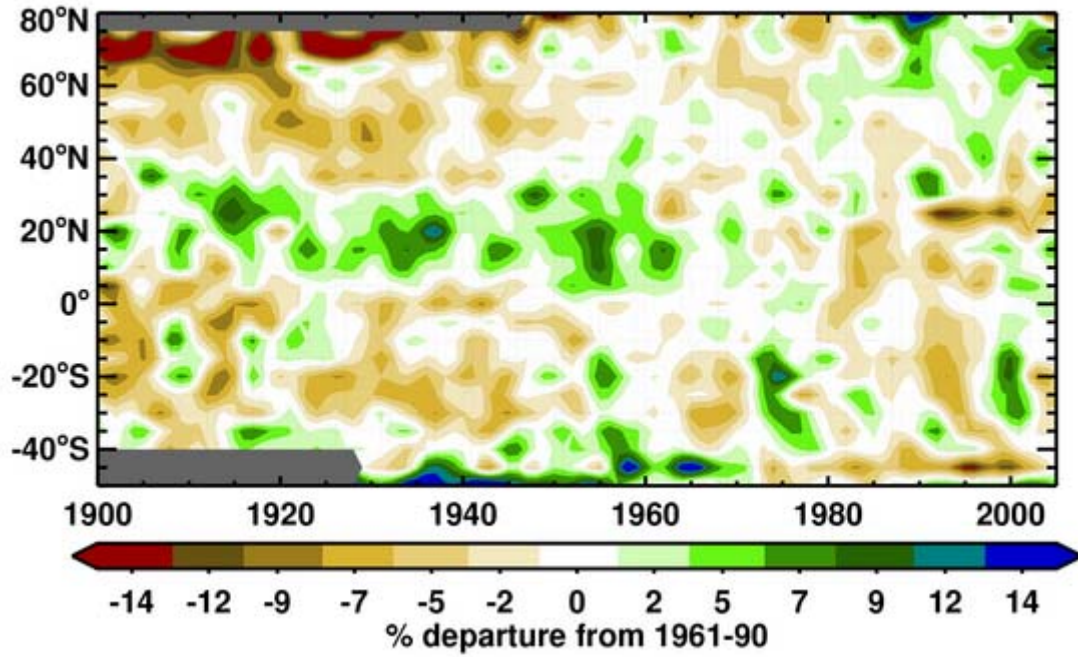
1



2

1 **Figure 3.3.3.** The centre figure is the annual mean trends % decade⁻¹, for 1900–2005. Areas in grey have incomplete data to produce reliable trends. The time series of annual
2 precipitation displayed (% of mean, with the mean given at top for 1961–1990) around the outside are for regions as given by name and indicated by the red arrow. The GHCN
3 precipitation from NCDC was used for the annual green bars and the black decadal curve, and for comparison the CRU decadal values are given in magenta. In most panels the range
4 is +30% to –30% except for the two Australian panels. The regions are those defined in Chapter 11.3.1 and include: Central North America, Western North America, Alaska, Central
5 North America, Eastern North America, Mediterranean, Northern Europe, North Asia, East Asia, Central Asia, Southeast Asia, Southern Asia, Northern Australia, Southern
6 Australia, Eastern Africa, Western Africa, Southern Africa, Southern South America, and Amazon.
7

1

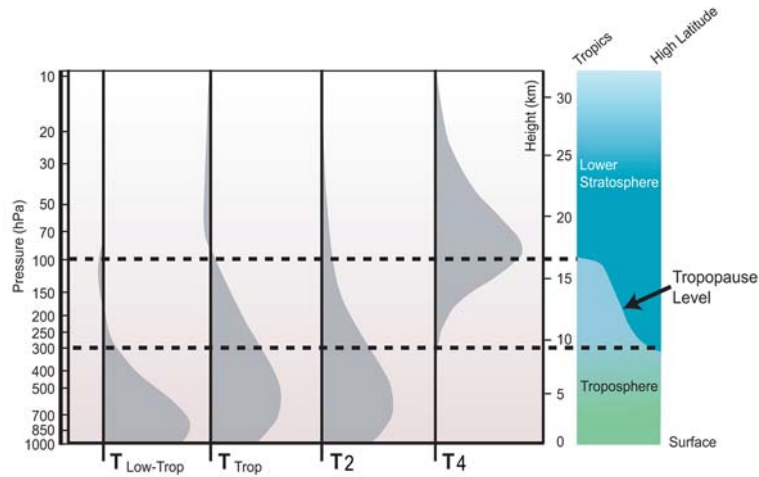


2

3

4 **Figure 3.3.4.** Latitude-time section of zonal average precipitation amount annual anomalies for land from
 5 1900 to 2005, relative to their 1961–1990 means (%). The values are smoothed with a 1/12(1–3–4–3–1)
 6 filter to remove fluctuations less than 6 years or so (see Appendix 3.A). The colour scale is nonlinear and
 7 white areas indicate missing.

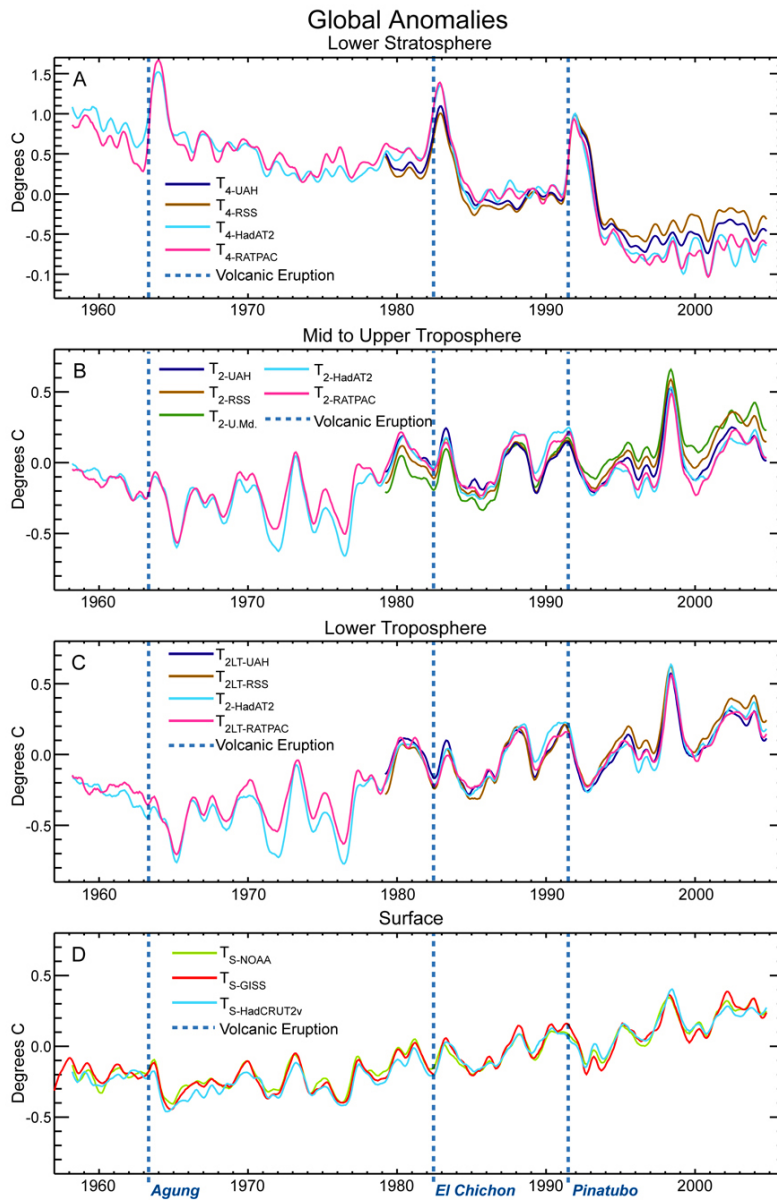
1
2



3
4
5
6
7
8
9
10
11

Figure 3.4.1. Vertical weighting functions depicting the layers sampled by satellite MSU measurements and their derivatives, and used also for radiosonde and reanalysis records. The right panel schematically depicts the variation in the tropopause from the tropics (left) to the high latitudes (right) and thus the dividing line between the stratosphere and troposphere. The fourth panel depicts T₄ in the lower stratosphere, the third panel shows T₂, the second panel shows the troposphere as a combination of T₂ and T₄ (Fu et al., 2004a), and the first panel shows T_{2_{LT}} from UAH for the low troposphere. Adapted from CCSP (2006).

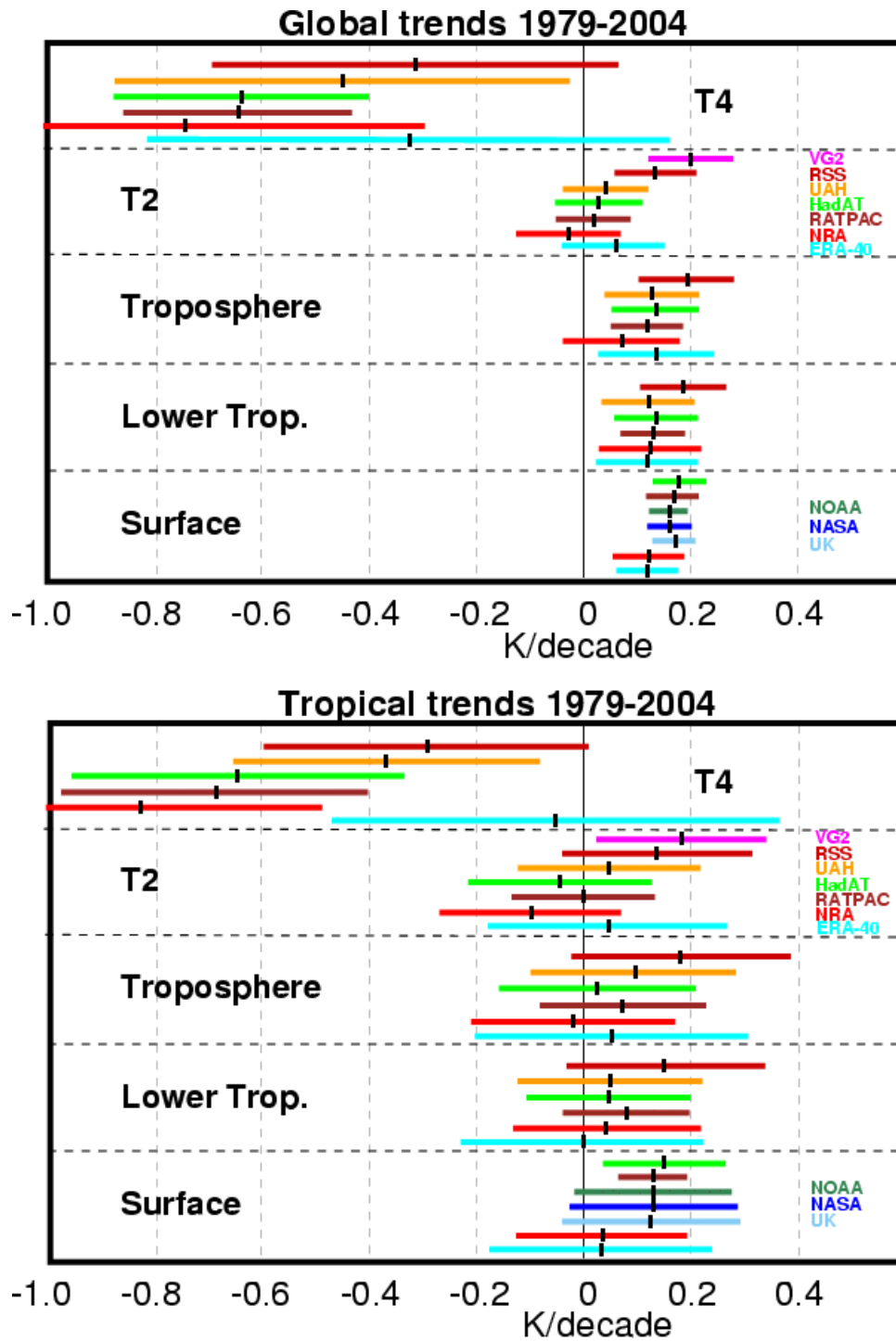
1
2



3
4
5
6
7
8
9
10
11

Figure 3.4.2. Observed surface and upper air temperatures. (A) Lower stratospheric T4, (B) Tropospheric T2, (C) Lower tropospheric T_{2LT} from UAH, RSS and VG2 (UMd) MSU satellite analyses, UKMO HadAT2 and NOAA RATPAC radiosonde observations; (D): surface records from NOAA, NASA GISS and UKMO/CRU (HadCRUT2v). All time series are based on monthly mean anomalies relative to 1979 to 1997 smoothed with a 7 month running mean filter. Times of major volcanic eruptions are indicated by vertical blue dashed lines. From CCSP (2006).

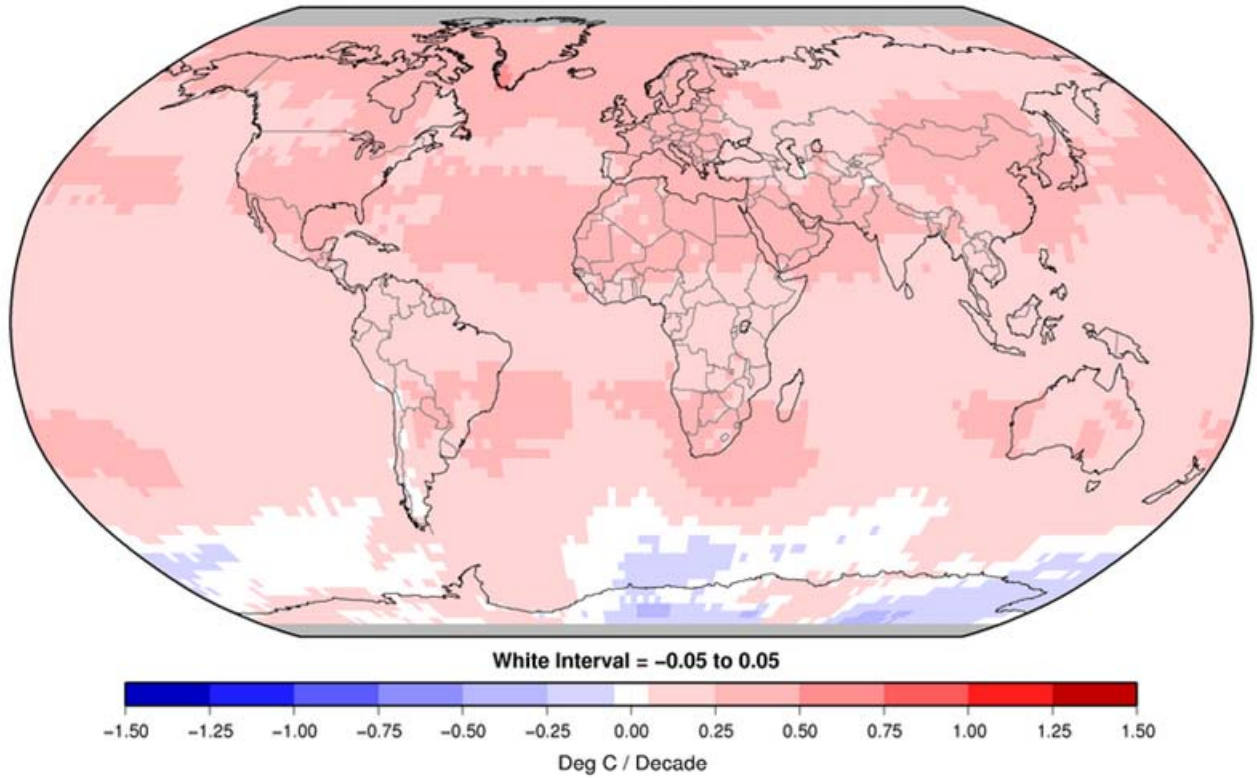
1



2
3

4 **Figure 3.4.3.** Linear trends of temperature ($^{\circ}\text{C decade}^{-1}$) for 1979–2004 for globe (top) and tropics 20°N –
 5 20°S (lower) for the MSU channels T4 (top panel) and T2 (second panel) or equivalent for radiosondes and
 6 reanalyses; for the troposphere (third panel) based on T2 with T4 used to statistically remove stratospheric
 7 influences (Fu et al., 2004a); the lower troposphere (fourth panel) based on the UAH retrieval profile; and
 8 the surface (bottom panel). Surface records are from NOAA/NCDC (green), NASA/GISS (blue) and
 9 UKMO/CRU (light blue). Satellite records are from UAH (orange), RSS (dark red) and VG2 (pink);
 10 radiosonde based records are from NOAA RATPAC (brown), and HadAT2 (light green); and atmospheric
 11 reanalyses are from NRA (red), and ERA-40 (cyan). Confidence limits are 95% (two standard errors)
 12 temporal sampling with an allowance for autocorrelation. Where the confidence limits exceed -1 , the values
 13 are truncated. ERA-40 trends are only for 1979 to August 2002. Data from CCSP (2006; from D. Seidel
 14 courtesy J. Lanzante, and J. Christy).

1
2

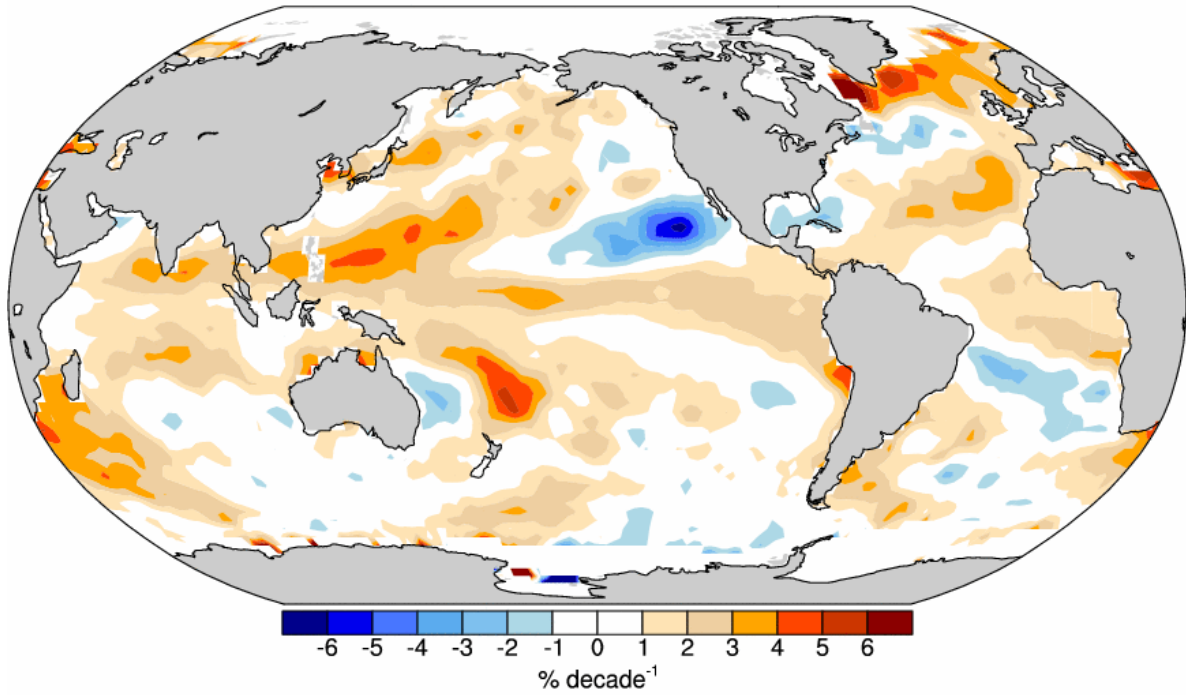


3
4
5
6

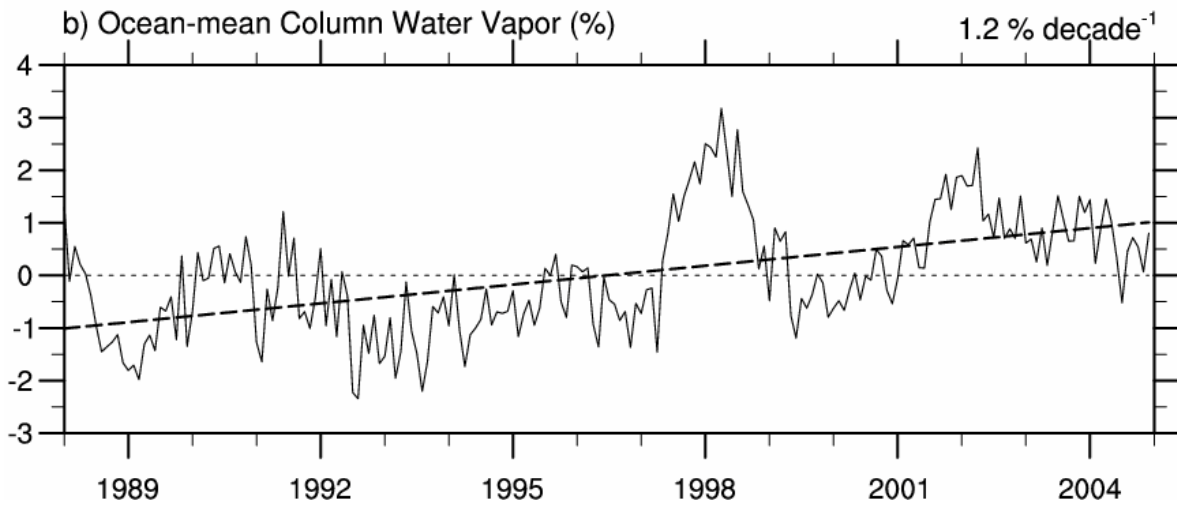
Figure 3.4.4. Linear trends of temperature for 1979–2005 for the troposphere from RSS (based on T2 and T4 adjusted as in Fu et al., 2004a) in °C decade⁻¹. Courtesy Q. Fu.

1
2

a) Column Water Vapor Trend 1988-2004 (% decade⁻¹, Ocean Only)



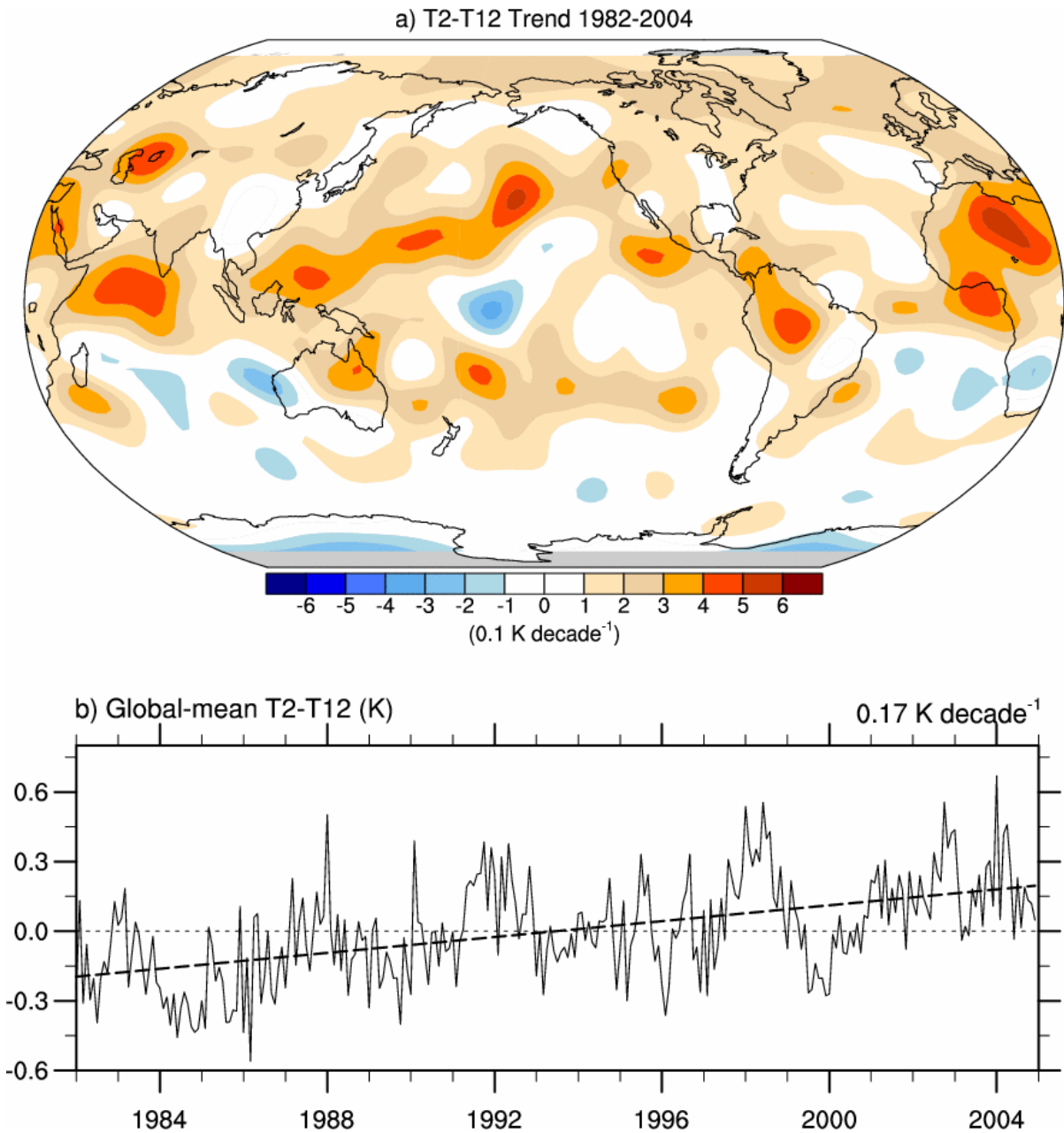
b) Ocean-mean Column Water Vapor (%)



3
4
5
6
7
8

Figure 3.4.5. Linear trends in precipitable water for 1988–2004 in % per decade (top) and monthly time series of anomalies over the global ocean plus linear trend (bottom), from RSS SSM/I (updated from Trenberth et al., 2005).

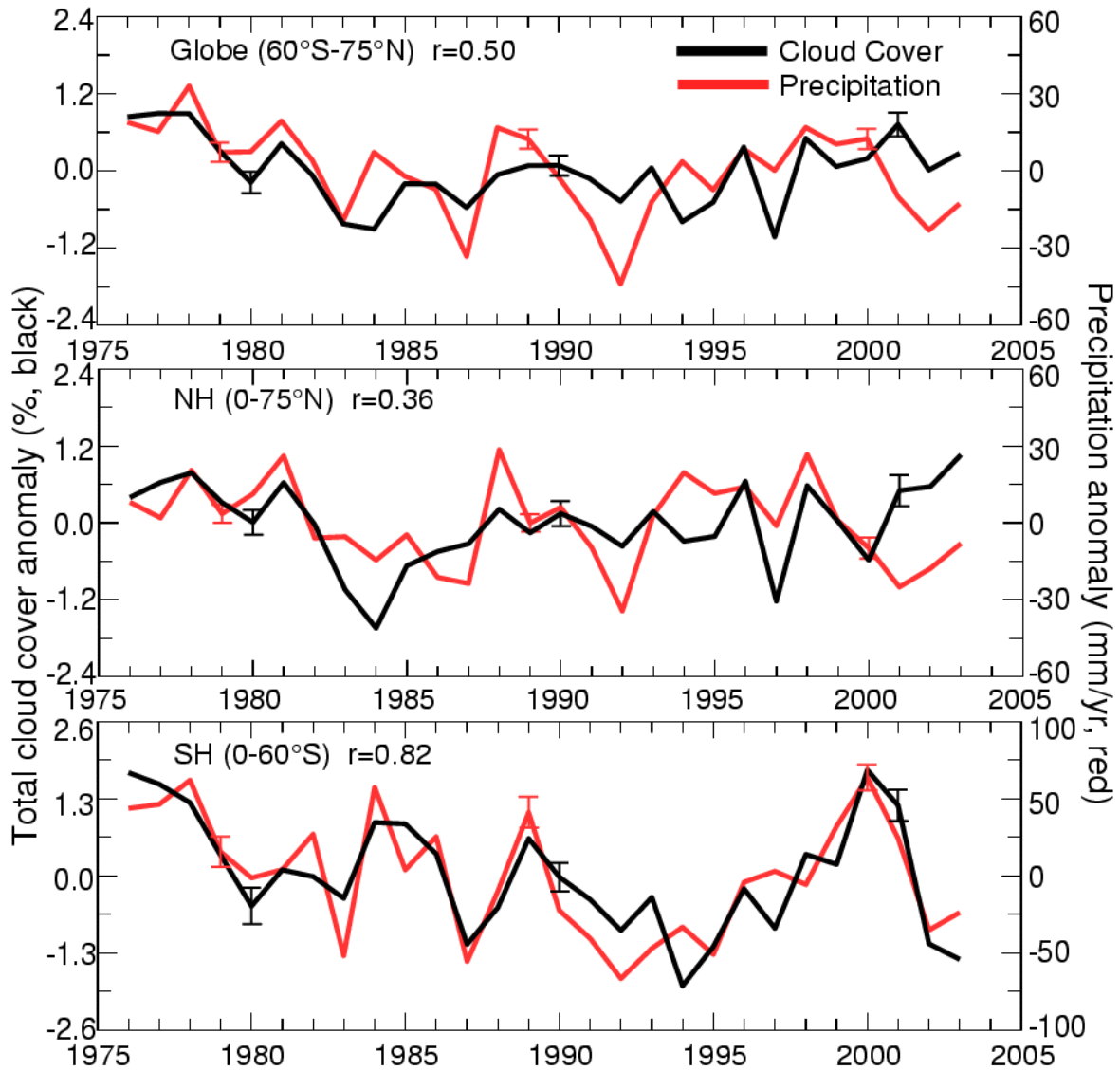
1



2
3
4
5
6
7
8

Figure 3.4.6. The radiative signature of upper tropospheric moistening is given by upward linear trends in T2–T12 for 1982–2004 in 0.1 K per decade (top) and monthly time series of the global-mean anomalies and linear trend (dashed) (bottom). Data are from the RSS T2 and HIRS T12 (Soden et al., 2005). The map is smoothed to T31 resolution.

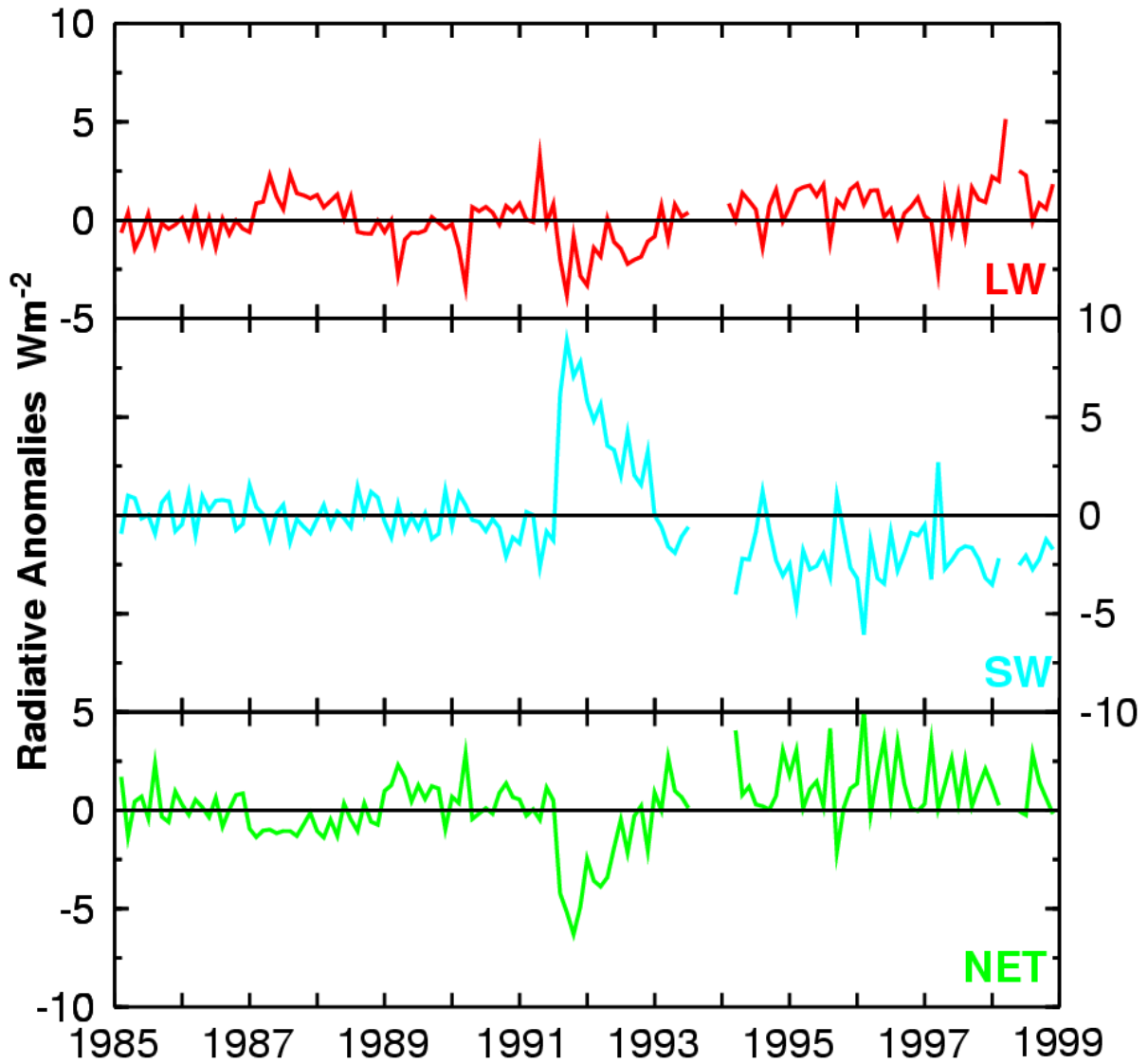
1
2



3
4
5
6
7
8
9
10

Figure 3.4.7. Annual total land (excluding the U.S. and Canada) cloud cover (black) and precipitation (red) anomalies from 1976 to 2003 over global (60°S–75°N), NH and SH regions, with the correlation coefficient (r) shown at the top. The cloud cover is derived by gridding and area-averaging synoptic observations and the precipitation is from Chen et al. (2002). Typical error bars for each decade are one standard error estimates using inter-grid-box variations (from Dai et al., 2006).

1
2



3
4
5
6
7
8
9

Figure 3.4.8. Tropical mean (20°S to 20°N) TOA flux anomalies for LW, SW, and NET radiative fluxes from 1985 to 1999 [NET = -(LW+SW)]. Coloured lines are observations from ERBS Edition 3_Rev1 data from Wong et al. (2006), updated from Wielicki et al. (2002a) including spacecraft altitude and SW dome transmission corrections.